analytical chemistry

Article

Cite This: Anal. Chem. 2017, 89, 6277-6284

pubs.acs.org/ac

Nondestructive Redox Quantification Reveals Glassmaking of Rare French Gothic Stained Glasses

Myrtille O. J. Y. Hunault,*[,†,‡,⊥] Claudine Loisel,*[,†] Fanny Bauchau,[†] Quentin Lemasson,[§] Claire Pacheco,[§] Laurent Pichon,[§] Brice Moignard,[§] Karine Boulanger,[∥] Michel Hérold,[∥] Georges Calas,[‡] and Isabelle Pallot-Frossard[†,§]

[†]Laboratoire de recherche des monuments historiques, CRCC, MNHN, USR CNRS 3224, Ministère de la culture et de la communication, 29 rue de Paris, 77420 Champs-sur-Marne, France

[‡]Institut de minéralogie, de physique des matériaux et de cosmochimie, Sorbonne Universités, UPMC, UMR CNRS 7590, 4 place Jussieu, 75005 Paris, France

[§]Centre de recherche et de restauration des musées de France, Palais du Louvre, 14 quai François Mitterrand, 75001 Paris, France

[∥]Centre André Chastel, Sorbonne Universités, Université Paris 4, 2 rue Vivienne, 75003 Paris, France

Supporting Information

ABSTRACT: The sophisticated colors of medieval glasses arise from their transition metal (TM) impurities and capture information about ancient glassmaking techniques. Beyond the glass chemical composition, the TM redox is also a key factor in the glass color, but its quantification without any sampling is a challenge. We report a combination of nondestructive and noninvasive quantitative analyses of the chemical composition by particle-induced X-ray emission−particle-induced γ-ray emission mappings and of the color and TM element speciation by optical absorption spectroscopy performed on a red-blue-purple striped glass from the stained glass windows of the Sainte-Chapelle in Paris, France, during its restoration. These particular glass pieces must have been produced as a single shot, which guarantees that the chemical variations reflect the recipe in use in a specific medieval workshop. The quantitative elemental mappings demonstrate that the colored glass parts are derived from the same base glass, to which TMs were deliberately added. Optical absorption spectra reveal the origin of the colors: blue from Co^{II}, red from copper nanoparticles, and purple from Mn^{III}. Furthermore, the derivation of the quantitative redox state of each TM in each color shows that the contents of Fe, Cu, and Mn were adjusted to ensure a reducing glass matrix in the red stripe or a metastable overoxidized glass in the purple stripe. We infer that the agility of the medieval glassmaker allowed him to master the redox kinetics in the glass by rapid shaping and cooling to obtain a snapshot of the thermodynamically unstable glass colors.

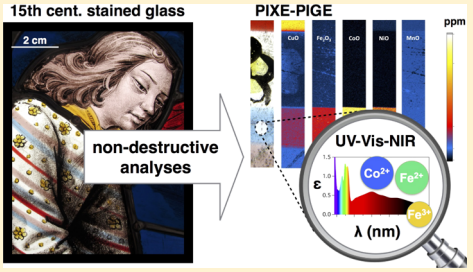

Stained glass windows are among the most impressive remnants of medieval heritage in Europe. A stunning example of the achieved colors is the 15th century apocalypse rose of the Sainte-Chapelle in Paris, France, a UNESCO World Heritage Monument (Figure 1a). These colors are obtained from specific transition metals (TMs).[1] The glass chemical composition and the fabrication conditions (furnace temperature and atmosphere) control the final coloration as it depends on TM speciation (coordination number and oxidation state). Therefore, the glass chemistry is a precious, and sometimes unique, testimony about glass history and glassmaking technology (origin, raw materials, and melting conditions). In particular, the quantification of the TM redox is a unique proxy of the fabrication process, as much additional information about the raw materials is blurred by the melting steps.

The question is how to use present-day analytical techniques to determine the glass chemistry and better understand the medieval glassmaking technologies.[2,3] Only a few studies of medieval glasses have discussed quantitatively the relation among the chemical composition, the quantitative speciation of the coloring elements, and the observed color. They have allowed the rediscovery of the fabrication technique of red glasses[4] or proved the specific reducing fabrication conditions of blue glasses[5] and other glasses.[6−8] Quantitative chemical analyses are crucial for building historical inferences from the comparison between different samples. Furthermore, the preciousness of stained glasses further requires nondestructive and noninvasive analytical methods. This is the purpose of the Accélérateur Grand Louvre d'Analyse Elémentaire (AGLAE) facility (Paris, France), which is dedicated to ion beam analysis of the chemical composition of ancient materials.[9] With regard to the determination of TM element speciation in glass, synchrotron-based X-ray absorption spectroscopy (XAS) techniques are the most used.[5,10−13] Besides, optical absorption spectroscopy (OAS) allows colorimetric study and provides unique information about the origin of the color,[1] with the

Received: April 19, 2017
Accepted: May 11, 2017
Published: May 11, 2017

DOI: 10.1021/acs.analchem.7b01452
Anal. Chem. 2017, 89, 6277−6284

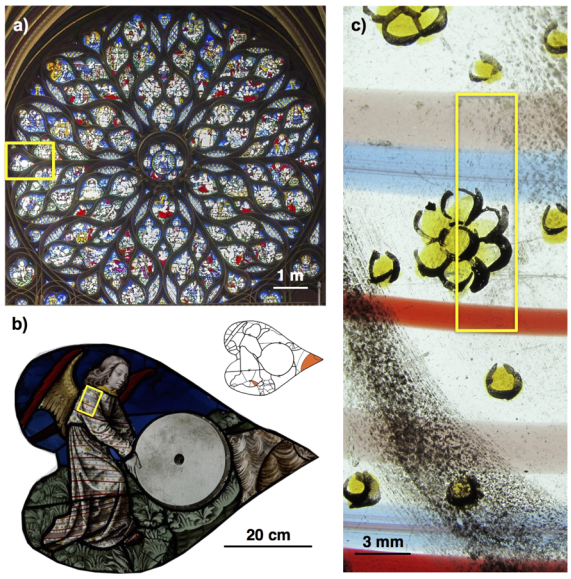

Figure 1. (a) Apocalypse rose of the Sainte-Chapelle in Paris. (b) Panel T9 containing the striped glass. The inset shows the historical dating of the glass pieces of panel T9 (white, original glass from the 15th century; orange, restoration glass from the 19th century). (c) Detail of the striped glass, where the area analyzed by PIXE and PIGE is highlighted by a yellow frame.

benefit of versatile portable setups.[14,15] However, the OAS analysis of the color of artworks has so far been mostly restrained to the visible energy range and to colorimetric data. Hence, one loses crucial information in particular regarding the contribution of Fe^{II} in the near-infrared (NIR) range,[1] which serves as a proxy of the melting conditions.[5,6] Recently, strong efforts were made to develop mobile optical absorption spectroscopmeters covering the entire ultraviolet (UV)−visible−NIR energy range and to apply OAS to the color analysis of stained glass windows as a nondestructive and noninvasive tool.[13−17] Furthermore, the derivation of quantitative information from OAS has been a challenge and has motivated several recent studies that compared XAS and OAS and assessed the quantitative determination of TM speciation with OAS.[5,13]

In this study, we report for the first time the combined nondestructive and quantitative determination of (i) the glass composition and homogeneity, using quantitative chemical mappings measured with particle-induced X-ray emission (PIXE) and particle-induced γ-ray emission (PIGE) at the AGLAE facility,[18−20] and (ii) the glass color and TM speciation, using OAS measured in transmission with a portable UV−visible−NIR setup.[15] We focus on a precious complex glass from the apocalypse rose of the Sainte-Chapelle in Paris, made of alternating blue, red, and purple glass stripes embedded in a colorless base glass (Figure 1b,c). The structure of this striped glass implies that these different colored glasses must have been melted in the same workshop and at the same time to allow their simultaneous handling and combination: potential differences in glass chemistry arise only from the recipes that were used in this workshop. Hence, this glass is an ideal and precise source of information about medieval glassmaking techniques. Coupled PIXE−PIGE chemical mapping and OAS allowed us to determine quantitatively the concentration and the speciation of the coloring TM elements without dismantling the panel or sampling the glasses, which should be avoided in general and was obviously impossible in the case presented here. The composition standard deviations are discussed according the glass inhomogeneities and origin. The TM concentration variations allow us to distinguish between impurities from the raw materials and TM added deliberately by the glassmakers to obtain each color from the same base colorless glass. These concentrations are used together with the OAS results and the glass thickness to calculate the Fe, Cu, and Mn redox. We propose and discuss the recipe used for each colored glass and the medieval glassmaking process that produced the striped glass. The recipe used for the silver-based yellow stain is also revealed.

EXPERIMENTAL SECTION

Stained Glasses. The glasses from this UNESCO-designated World Heritage site show the apogee of color mastering by medieval glassmakers. This stained glass window from the French flamboyant gothic period was built in 1493−1498 to replace the former degraded rose from the 13th century. It results from the most advanced glassworking techniques: high glass quality showing little degradation and engraved flashed colored glasses made of two or more layers of glass that induce complex coloring effects equivalent to the details obtained in oil painting.[21] However, as all archives were lost, neither the glass manufacturer(s) who fabricated the glass and its geographical origin nor the glazier/artist who created the windows by cutting, painting, and assembling the glass pieces with a leaded frame is known. The restoration of the apocalypse rose of the Sainte-Chapelle in Paris in 2014−2015 offered a unique opportunity to investigate the chemistry of these glasses with nondestructive analyses. Panel T9 contains an original multicolored striped glass from the 15th century (Figure 1b, inset). A few other similar striped glasses have been found in the apocalypse rose and in other churches in France and Europe (Figure S-1). This type of glass is sometimes termed Venetian or "*à-la-façon-de-Venise*" by analogy with the striped glass tableware produced on Murano island at that time.[22] This one was analyzed after careful cleaning conducted by the restorers. The striped glass sample was studied as is, embedded in the leaded framework. The thickness of the glass was measured using an ultrasonic thickness gauge at the spots where the measurements were taken.

PIXE−PIGE Chemical Composition Analysis. The elemental composition of the striped glass was analyzed using particle-induced X-ray emission (PIXE) and particle-induced γ-ray emission (PIGE) techniques, which allow quantitative chemical composition analysis. Elemental imaging capabilities have been developed at the AGLAE facility and were used in this study to scan a total surface of 3 mm × 19 mm from both sides of the striped glass. The 3 MeV proton beam was focused to 40 μm on the target. The scanning system that combined a vertical magnetic scan of the beam with a horizontal target translation allowed acquisition of one map for each side of the panel. One map results from a step-by-step scan, with a vertical step size fixed to 25 μm. PIXE data were acquired with four fast counting SDD X-ray detectors.[19] One detector flushed with He gas and protected from backscattered protons by a magnetic deflector was dedicated to measure low-Z (major) elements. For the measurement of trace elements, the system had three detectors to improve the statistics, which were screened with a 50 μm thick Al absorber to measure elements down to titanium. Lighter elements such as Na and F were investigated by PIGE using a HPGe γ-ray detector. With an intensity of 7

DOI: 10.1021/acs.analchem.7b01452
Anal. Chem. 2017, 89, 6277−6284

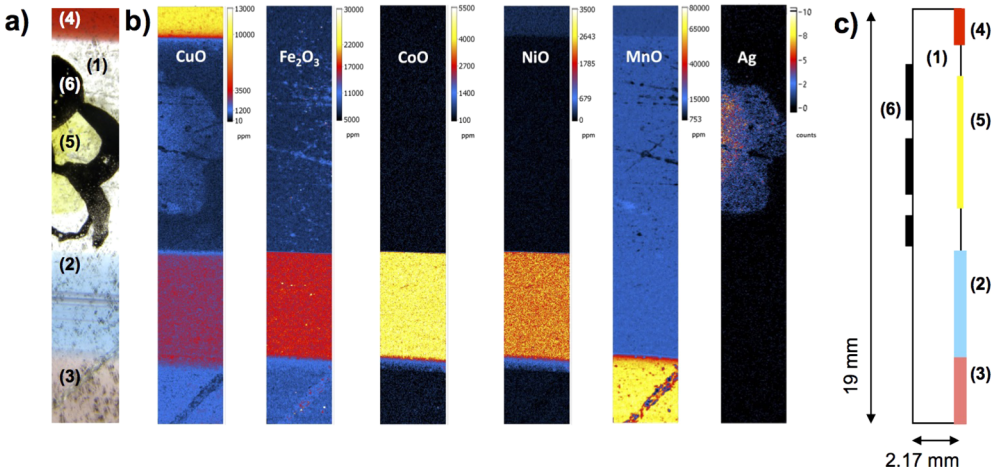

Figure 2. (a) Macrophotography of the analyzed area. (b) Quantitative chemical mappings of the main transition metal elements on the exterior face of the glass, revealing the colored stripes [blue (2), purple (3), and red (4)] and the yellow flower shape (5). (c) Scheme of the structure of the sample.

nA, the counting rates were 10−15 × 10^3 counts/s in the low-energy detector and 15−40 × 10^3 counts/s for the trace detectors. The total acquisition time was 3.5 h for each map. The charge was monitored by recording silicon X-rays emitted by the Si_3N_4 exit window with a dedicated EDX-SDD detector. AGLAEMap software[20] was used to visualize and process the raw maps. For each pixel, two PIXE spectra corresponding to low-energy and high-energy detectors and one PIGE spectrum were extracted. AGLAEMap software provides the possibility of grouping pixels or selecting only part of the initial map and thus deriving an average concentration over a selected area. We extracted in this way the spectra corresponding to each colored glass and base glass areas, to the yellow area, and to the *grisaille* paint. Sum spectra and PIXE maps were afterward processed using TRAUPIXE software,[18,20] based upon GUPIX software,[23] to obtain the quantitative mapping of the chemical compositions of the different glasses and of the paintings. The results of the PIXE analyses can be affected by the variation of the chemical composition across the sample thickness, especially in the presence of deteriorated glass layers. Here, the excellent state of preservation of the glass, showing very little surface corrosion, allows us to confirm that the concentration of mobile cations such as K^+ is representative of the bulk glass. In the case of Na^+, which can also be leached out of the glass by weathering,[24] it is probed only in the first micrometers of the sample depth by PIXE. On the other hand, PIGE allows us to probe further the bulk material, and thus, we give the concentration derived from PIGE for Na.[25] The depth of penetration depends on the chemical composition of the analyzed material. Here in the case of the glass presented here, it is estimated to be ∼80 μm.[26] These techniques allow selection of ideal areas without too much alteration, or paintings as well as rare glasses pieces presenting a complex fabrication process as in the case presented here.

Optical Absorption Spectroscopy. The optical absorption spectroscopy measurements were achieved in parallel to the chemical analysis on the same glass pieces, using a portable mobile setup based on an optical fiber pathway and CCD spectrometers as described elsewhere.[15] The optical absorption spectra were measured in transmission over the 350−2500 nm energy range. The beam size on the sample was <1 mm^2 and allowed selection of a precise spot free of surface alteration and paintings for analysis. Optical absorption A is given by the Beer−Lambert law: $A = d\sum_i(c_i\varepsilon_i)$, where ε_i (liters per mole per centimeter) is the molar extinction coefficient of absorbing species i and d is the thickness of the sample measured using the ultrasonic thickness gauge. The concentration of the absorbing species, c_i (moles per liter), is obtained from chemical analysis of the glass and the density of the glass. Density ρ_i (grams per cubic centimeter) of the glass samples was estimated to be 2300 g cm^{-3} from model potash lime silicate glasses using the Archimedean method. Colorimetric analysis was performed by computing the CIE values of L^*, a^*, and b^* (unitless) of the colorimetric system defined in 1976 by the International Commission on Illumination. The colorimetric CIE values of L^*, a^*, and b^* are calculated using D65 illuminant and CIE 1931 2° observer.[27] L^* describes the luminosity of the color (0, black; 100, white), and a^* and b^* describe the color hue: a^* varies from −120 (green) to 120 (red), and b^* varies from −120 (blue) to 120 (yellow). The higher the absolute values of a^* and b^*, the more saturated the color.

RESULTS AND DISCUSSION

Chemical Compositions: Geographical Origin of the Glass. The chemical compositions of the different parts of the striped glass were extracted from the PIXE and PIGE chemical mappings (Figure 2a and Table S-1). The major oxide contents (Na_2O, K_2O, CaO, MgO, Al_2O_3, and P_2O_5) are very similar between the colored stripes and the colorless base glass (Table S-1). Alkalis and alkaline-earth ions come from the plant ashes that are added to lower the melting point of the silica of the sand.[28] The low Na_2O content (<1.13 wt %) and the high CaO (>13.83 wt %) and K_2O (>15.86 wt %) contents in the base glass reveal a "potash" type glass composition.[29] These elements result from the raw materials used to make the glass. Their respective concentrations assess here the use of continental plant ashes made from ferns, oak, or beech and not from coastal plants.[30,31] The low PbO concentration (<0.24 wt %) attests that the glass used here is not lead glass, which can usually contain up to 18 wt % PbO.[32] Because the three colored glasses are embedded in the same base glass pieces, these glasses must have been melted in the same workshop and at the same time to allow their simultaneous handling and

DOI: 10.1021/acs.analchem.7b01452
Anal. Chem. 2017, 89, 6277−6284

combination. This hypothesis is further supported by the very close chemical compositions for the major elements. Therefore, the comparison between the major element compositions of these glasses should provide unique information about the variation of composition within the same workshop over a very short time period.

Standard deviations present key information about the variation of the chemical composition and to what extent the variation can be interpreted in terms of a different batch recipe. Such information is essential for arguing whether a corpus of samples belongs to the same workshop. The calculated standard deviations of the measured chemical compositions are listed in Table 1. We distinguish two factors that influence these values: (i) the statistical error of the measurement defined as the repeatability, which was determined on a reference material (glass Brill D),[33,34] and (ii) whether considering a series of analyses on different points of a historical glass sample, the obtained standard deviations include the statistical error and the variation due to the heterogeneity of the sample. These standard deviations were calculated from a series of three punctual analyses and on a series of three submaps on the base glass. The obtained standard deviations are larger than the statistical error. Furthermore, the standard deviations obtained from three submaps are larger than from punctual analyses, quantifying the relative heterogeneities of the glass.

Table 1. Relative Standard Deviations Calculated for Different Series of Three Measurements Comparing the Factors That Influence the Chemical Composition Variations (PIGE)

	Na_2O	MgO	Al_2O_3	SiO_2	P_2O_5	K_2O	CaO
				Repeatability[a]			
Brill D	2.1%	1.3%	1.0%	0.2%	1.3%	0.5%	0.8%
				Sample Heterogeneity			
punctual	5%	1%	1%	1%	1%	1%	1%
mapping	4%	3%	2%	1%	1%	2%	2%
				Workshop Variation[b]			
four colors	14%	4%	6%	1%	3%	4%	7%

[a]Estimated from the reference material glass Brill D.[33] [b]After renormalization of the composition including only the major oxides.

The base glass and the colored glasses were necessarily melted in different pots (ceramic containers for the melted glass in the furnace[28]). The variations in composition among the base glass, the blue stripes, and the red stripes are listed in Table 1. Although the compositions are very similar, the calculated relative standard deviations are larger than those due to statistical error and heterogeneities. This suggests that a similar recipe was used for the glass for each pot (base glass and colored glass) but that some variations occurred probably because of errors when weighing the components. However, we note that the relative standard deviations are small compared to those reported for other medieval glass corpora.[29] In fact, a sample corpus results usually from the collection of various glass pieces from excavations or a window panel, with no indication that they belong to the same workshop or were produced at the same time. Our results suggest that the ancient fabrication process in use in a workshop on a given day was accurate enough to produce a relatively constant glass chemical composition in terms of major oxides, a crucial criterion for maintaining the constant temperature−viscosity behavior of the glass and allowing its processing.

The chemical composition results allow us to form three important interpretations. (i) They confirm that all four glasses were made in the same workshop. Similar concentrations of trace elements such as Zr and Ti (Table S-1), within standard deviations, suggest that all the glasses composing this striped glass were prepared from the same raw materials. (ii) Potash-lime type chemical composition rules out the fabrication in Venice, or "*à-la-façon-de-Venise*" in Northern Europe from emigrated Venetian glassmakers. Venetian glasses were soda-rich as they were made of soda-rich plant ashes (>10 wt % Na_2O).[35] On the other hand, it supports a Northern France origin, with the use of wood ashes.[29,36] (iii) A similar composition is crucial for allowing similar thermal expansion coefficients to prevent the striped glass from breaking when it is cooled. The chemical mappings of both sides of the glass reveal that the colored stripes are included at the surface of the base glass on the outdoor side as illustrated in the cross-section scheme (Figure 2c). The correlation between the colored glass stripes and the TM (Mn, Fe, Co, and Cu) concentrations highlights that transition metal oxides were added to induce the color of the respective glass batches.

In the base colorless glass, Fe and Mn are the main TM elements (Table S-1). Iron is a common impurity of the sand and raw materials, and the concentration measured in the base glass agrees with the concentrations reported for other medieval glasses.[9] The optical absorption spectrum of the base glass (Figure 3) shows a large absorption band centered at ~10000 cm^{-1} assigned to Fe^{II}.[1] The colorimetric L^*, a^*, and b^* coordinates for the base glass are listed in Table 2. The high L^* value attests to the relatively high transparency of the glass. The negative a^* and positive b^* values, close to zero, attest to the green-yellowish pale hue. According to the measured glass

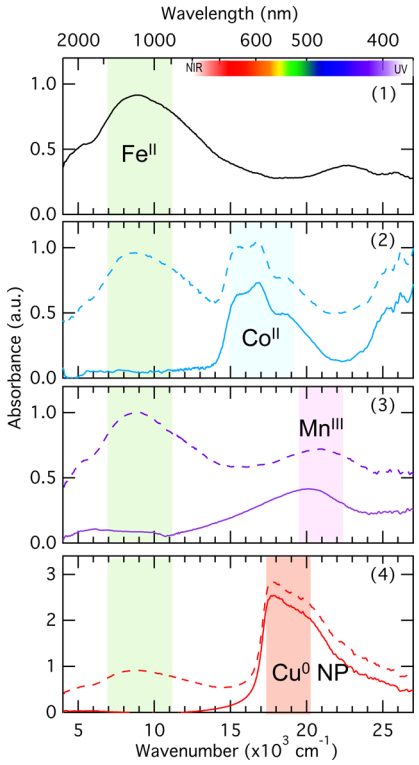

Figure 3. Optical absorption spectra of the different parts of the glass, labeled 1−4 according to Figure 2a. Colored solid line spectra result from the subtraction of the colorless base glass spectrum (1).

DOI: 10.1021/acs.analchem.7b01452
Anal. Chem. 2017, 89, 6277−6284

Table 2. Colorimetric CIE L^*, a^*, and b^* Values for Each Part of the Analyzed Striped Glass

glass color	material	L^*	a^*	b^*
colorless	base glass	68.9	68.9	5.6
blue	glass stripe	41.1	41.1	−23.3
purple	glass stripe	42	42	3.1
red	glass stripe	18.7	18.7	4.1
yellow flower	paint	54.1	54.1	39.1

thickness (2.17 mm, which is close to the lower bound of observed medieval glass thickness values), the Fe concentration (7600 ppm as total Fe_2O_3), and the molar absorption coefficient of Fe^{II} at 10000 cm^{-1} ($\varepsilon[Fe^{II}]$ = 25 L mol^{-1} cm^{-1}[11]), we estimate using the Beer−Lambert law that 60% of the Fe is divalent. Low-intensity features observed at 22000−23000 cm^{-1} may be assigned to Mn^{II} and Fe^{III}, while no Mn^{III} is detected at 21000 cm^{-1}.[1] Although manganese can be an impurity associated with the sand used for the glass, it is well-known from ancient (Theophilus's treatise[37]) and modern (Georges Bontemps's treatise[38]) glassmakers, and has been assessed by successive studies,[7,39] that manganese was intentionally added to counterbalance the redox equilibrium of iron and correct the greenish color that ferrous iron impurities give to the glass (also known as "glassmaker's soap"). These aspects will be discussed further below. The blue stripe area on the chemical mappings (Figure 2 b) corresponds to the highest concentration of CoO (0.39 wt %) and NiO (0.21 wt %) and a relatively high concentration of CuO (0.26 wt %) (Table S-1). No Co−Zn−Pb−In correlation or Co−Sb correlation was found, which rules out the use of Co ore from Freiberg mines (Germany) or the Middle East. Therefore, cobalt was probably intentionally added from German *saffera*, a cobalt-rich ore, as mentioned by ancient treatises.[40] It correlates with the presence of arsenic (120 ppm), suggesting that cobalt ore was probably obtained from the mining district of Schneeberg (Germany). The optical absorption spectrum of the blue stripe (Figure 3) reveals the typical triple absorption band of Co^{II} at 15500, 16770, and 18500 cm^{-1} in the visible range [$^4A_{2g}$ (^4F) → $^4T_{1g}$ (^4P), T_d symmetry], confirming that the observed blue color is due to Co^{II} as the main coloring species.[5,41] The expected NIR triple absorption band [$^4A_{2g}$ (^4F) → $^4T_{1g}$ (^4F)] superimposes with the broad band identified as originating from Fe^{II}. The comparison with the spectrum of the base glass reveals that the NIR Fe^{II} band arises mainly from the base glass contribution, and this contribution can be subtracted from the spectrum of the blue glass to obtain only the spectrum of the blue stripe. In the corrected spectra from base glass absorption, it is not possible to distinguish the contribution from either Fe^{II} ions or Cu^{II} (blue) ions,[1] both expected to be around 10000 cm^{-1}, suggesting that the contribution of the additional Fe and Cu ions in the blue glass is negligible.[5] Assuming that the maximal molar absorption coefficient of Co^{II} ($\varepsilon[Co^{II}]$) equals 180 L mol^{-1} cm^{-1} in this potash-lime type of glass matrix,[41,42] we estimate the thickness of the stripe to be 0.39 mm.

The highest concentration of manganese (7.19 wt % MnO) is found in the purple stripe (Figure 2b). An earth-abundant mineral known to be used as a source of manganese is pyrolusite (MnO_2). Here, the concentration of manganese is correlated with the presence of barium (Figure S-2), which suggests that psilomelane [$(Ba,H_2O)_2Mn_5O_{10}$] was also present in the ore used as a source of manganese. However, the very high MnO concentration in the purple glass is nonlinearly correlated to the BaO content in the other colors. It suggests an addition from a source of manganese different from the one used as "glassmaker's soap". The optical absorption spectrum of the purple stripe (Figure 3) shows an intense large asymmetric absorption band around 21000 cm^{-1} assigned to Mn^{III}. The spectrum corrected for the absorption of the base glass shows that no Fe^{II} is present in the purple stripe (Figure 3). Assuming that the thickness of the purple stripe is similar to that calculated for the blue stripe, we estimate from the manganese concentration that 10% of the total Mn content is in the trivalent state ($\varepsilon[Mn^{III}]$ = 25 L mol^{-1} cm^{-1}[42]). The red stripe correlates with the highest concentration of copper (1.06 wt %) (Figure 2b). The optical absorption spectrum reveals the typical intense and abrupt absorption rise assigned to the surface plasmon resonance (SPR) at 17700 cm^{-1} (565 nm) (Figure 3) from Cu metallic nanoparticles (NPs)[1,4,43,44] and agrees with the highly saturated red color evidenced by the high a^* value. This is analogous to the gold-ruby glasses colored by gold NP.[43,45] The amount of MnO in the red stripe glass is significantly lower (0.93 ± 0.02 wt % MnO) than in the base and blue glasses (1.19−1.28 ± 0.05 wt % MnO) (Table S-1 and Figure S-3). These results lead to three hypotheses. (A) Variations in the MnO content arise from the use of different sand batches that contain different amounts of manganese impurities. However, according to the compositions of Ti and Zr impurities that are markers of the used sand, it is most probable that the same sand was used for all the glasses analyzed here. (B) The MnO concentration in the red stripe is the minimal concentration arising from the manganese impurities contained in the sand, and the difference with the base and blue glasses arises from a voluntary addition by the glassmakers. (C) The MnO content in all three glasses results from a voluntary addition by the glassmakers. This is supported by the almost linear relation between the concentrations of MnO and BaO in the red, blue, and base glasses. The measured variation would result from either the empirical imprecision in the recipe or the addition of a precise and careful amount to control the final color.

The observed colors depend on redox equilibria controlled by the oxygen activity in the glass, which depends on the chemical composition, temperature, partial pressure of oxygen, and TM concentrations.[46] The redox equilibria can further interfere together, and their relative reactivity in glass has been extensively investigated. Figure 4 shows the fraction of the reduced species of a given redox couple as a function of the partial pressure of oxygen of the furnace atmosphere. In the colorless base glass, the presence of both Fe and Mn controls the glass color according to the equilibrium Fe^{II} (green) + Mn^{III} (purple) → Fe^{III} (yellow) + Mn^{II} (colorless). The "glassmaker's soap" ($Mn^{III,IV}$ oxides, such as pyrolusite or psilomelane) was added to shift to the right the equilibrium mentioned above, hence removing the greenish coloration arising from the presence of Fe^{II}. The redox estimation for iron and manganese correlates with a partial pressure of oxygen in the furnace atmosphere of ∼10^{-7} bar (Figure 4), in agreement with values reported for medieval blue glasses.[5] At this partial pressure of oxygen, Schreiber's diagram (Figure 4) confirms that all Mn ions are present as reduced Mn^{II}, which does not give any color (the $3d^5$ high-spin ion gives no spin-allowed optical transition possible from the $^6A_{1g}$ ground state in O_h symmetry). In the blue glass stripe, although the control of the iron redox is not necessary because the strong Co^{II} colorant dominates the final color, the similar MnO content compared to that of the base

DOI: 10.1021/acs.analchem.7b01452
Anal. Chem. 2017, 89, 6277−6284

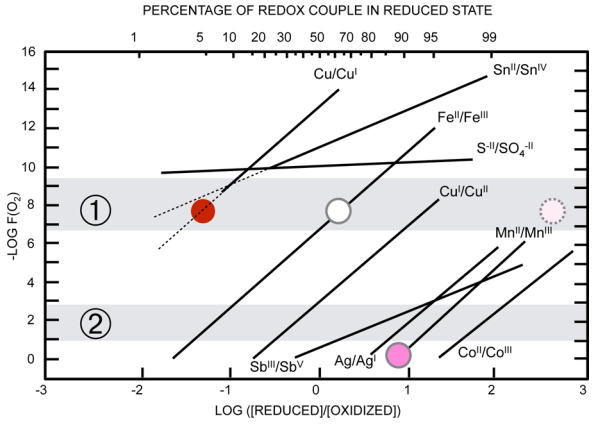

Figure 4. Fraction of the redox couple in the reduced state as a function of the oxygen partial pressure at 1150 °C. ① Medieval furnace atmosphere.[5] ② Air. Colored dots correspond to the redox estimated for the corresponding colored glass stripe. Adapted from refs 46−48.

glass suggests that the same recipe as that used for the base glass was used. The estimation of the redox state of Mn ions in the purple glass corresponds to an effective oxidant partial pressure of oxygen (10^{-1} bar) in the furnace atmosphere, which was certainly not achieved in medieval furnaces and is incompatible with the speciation observed in the base glass. This suggests that Mn redox is in a metastable overoxidized state and that the exceptionally high manganese concentration was used (i) to compensate for the presence of Fe^{II} that reduces Mn^{III} and therefore all Fe^{II} has been oxidized into Fe^{III} and (ii) to anticipate the discoloration during the manipulation of the fused glass due to the thermodynamic reduction to Mn^{II} toward the equilibrium (Figure 4). The kinetics of the reduction relies on the diffusion of oxygen in the glass and stresses the importance of rapid glass shaping and justifies the high manganese concentration. Obtaining the ruby-red color was another challenge for medieval glassmakers. As in the case of gold ruby glass,[43] the first stage of the process required preparation of a glass containing monovalent ion Cu^{I} (colorless) and then inducing the reduction of Cu^{I} to insoluble Cu^{0}, which precipitates as metallic copper nanoparticles.[4,43] Cu^{I}-rich glass agrees with the partial pressure of oxygen of the base glass (Figure 4) and is supported by previous XANES results.[10,49] The lower MnO concentration in the red stripe than in the base glass and the other stripes confirms that a specific glass batch with no extra oxidative Mn was added to the red glass (Figure S-3). This supports the hypothesis B given above. As for other medieval red glasses,[4] the absence of significant amounts of reducing elements[43,46] suggests that the reduction to metallic copper arises only from the thermodynamically favored small fraction of metallic copper. An annealing step at a temperature slightly below the glass transition temperature favors the diffusion of the loose Cu^{I} ions and allows the nanoparticle growth by Oswald ripening until it gives the red color.[43,50,51]

Painted Decorations. The striped glass shows, in addition to the colored stripes, a fine yellow and black flower painting that was achieved by the glazier who bought the glass to create the window. This is further observed in the chemical mappings of Ag and Cu on the outdoor side (Figure 2b,c) and Fe, Cu, and Pb on the indoor side of the glass (Figure S-4), which correlate with the flower shape. The chemical composition of the yellow flower area differs from the base glass composition in only the concentration of Ag (2500 ppm), which suggests that the yellow color arises from the use of a silver-based paint and the resulting Ag absorbed into the glass matrix. The optical absorption spectrum of the yellow stain was measured on the collar of the angel character and is given in Figure 5. It shows

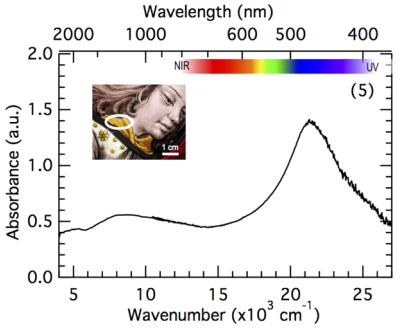

Figure 5. Optical absorption spectrum of the yellow staining on the collar of the angel (inset).

an intense (1.8 au) peak at 21300 cm^{-1} (470 nm) assigned to the plasmon peak resonance of metallic Ag nanoparticles.[52−55] The average size of the nanoparticles can be derived from the shape of the plasmon resonance, using[56] the equation $R = V_f\lambda_p^2/(2\pi c\Delta\lambda)$, where R is the average radius of the metallic clusters, V_f is the Fermi velocity of the electrons in bulk metal (for Ag, $V_f = 1.39 \times 10^8$ cm s^{-1}), λ_p is the peak position of the resonance, $\Delta\lambda$ is the full width at half-maximum (fwhm) of the absorption band (here 90 nm), and c is the speed of light. We find that the Ag nanoparticle average size should be between 1 and 2 nm, in agreement with previous studies.[16,54] Altogether, this reveals that the yellow flower was painted on the external face of the glass with yellow silver stain, a painting technique developed in the 14th century. The resulting color shade and intensity depends on the silver stain composition, and a comparison of the absorption intensity and colorimetric values (Table 2) with previous results[54] suggests that in the case presented here the stain was made with clay (kaolinite). This agrees with one of the recipes described in the treatise from Antoine de Pise (14th century) based on crushed metallic silver mixed with ochre.[55,57] The resulting mixture is applied with a brush on one side of the glass. Then a firing step induces the oxidation of silver and migration of the silver ions in the first few micrometers of the glass.[55] The clay used as a binder has little interaction with the glass and is removed afterward. The migration of the Ag^{I} ions in the glass is followed by immediate reduction and nucleation of NPs, in agreement with the high redox potential of the Ag^{0}/Ag^{I} couple and poor solubility of Ag^{0} in the glass. The black stain *grisaille* is an opaque brown-black vitreous painting used to make black drawings by blocking light transmission. The chemical composition of the *grisaille* was extracted from the most iron-concentrated, and thus thickest, area of the chemical mappings (Figure S-4) to avoid interference with the support glass composition. Iron oxide is highly concentrated (25.56 wt % total Fe_2O_3), while the silica, potassium, and calcium fractions are smaller than in the base glass (Table S-1). We further note the important concentration of PbO (8.5 wt %). Altogether, this composition agrees with the recipe reported: *grisaille* is obtained by grinding iron oxide and lead silicate glass.[58] After firing, the resulting *grisaille* is a heterogeneous layer bound to the support glass and composed of a glass matrix and oxide inclusions as confirmed by the large

DOI: 10.1021/acs.analchem.7b01452
Anal. Chem. 2017, 89, 6277−6284

standard deviations (Table S-1). The presence of paintings of the glass attests that a last firing step was performed in the glazier workshop to make the stained glass window. Both firing steps for yellow silver stain and *grisaille* stain were performed at similar temperatures (just below the glass transition temperature of 630 °C[59]) in a furnace, which allowed to proceed both firing simultaneously. Some cases show that *grisaille* and yellow silver stain were applied on the same side of the glass.[60] However, it was reported that when clay is used in the preparation of the yellow silver stain, then it is incompatible with the *grisaille*.[57] This explains why the yellow silver stain and the *grisaille* are painted on opposite faces of the striped glass as illustrated in Figure 2c. The presence of the *grisaille* on the indoor face of the glass agrees with usual practice reported in glazing techniques to minimize weathering.

Glass Fabrication. Wrapping together the results obtained on the glass chemical composition and the redox estimations, we can infer interpretations of how this glass was made as summarized in Figure 6. First, a glass batch was prepared from the raw materials in use in the medieval France area, leading to a potash type composition (①). This initial glass has a greenish color because of divalent speciation of iron impurities in a reducing furnace atmosphere. Part of this initial batch has probably been used to prepare the red glass (②). The red color is obtained by adding copper. The rest of the batch was added with "glassmaker's soap" manganese oxides to oxidize Fe^{II} and remove the greenish color. This is the base glass. A small part of this colorless batch was then probably used to make the blue and purple glass batches (③). The blue color was obtained easily by adding cobalt ores (④). The purple color was obtained by adding manganese ores in large amounts (⑤). The French origin of this glass postulated according to the potash-lime matrix composition suggests that the striped glass was blown in analogy with double-layer flashed glasses (⑥): strings of melted colored glass were rolled around the base colorless glass bubble attached to a blowing cane before being blown altogether in a single shot. The preparation of the purple and red glass batches must have been synchronous, and the entire blowing process of the striped glass must have been a rapid process handled by skilled glassmakers. There was striking thermodynamic antagonism between the reduced copper red and the oxidized manganese purple colors, while the glass was handled and annealed under similar conditions (below ~630 °C[59]), several times: after the glass had been blown to obtain the glass sheet and then for the purpose of black *grisaille* and yellow silver stain (⑦). It reveals that TM concentrations must have been precisely adjusted to allow the colors of the stripes to be stable enough to resist other firing steps. The stability of both colors suggests that the formation and growth of the copper nanoparticles in the red glass are limited by Cu diffusion in the glass,[4] while the discoloration of the purple glass is limited by the high glass viscosity around the transition temperature.[59]

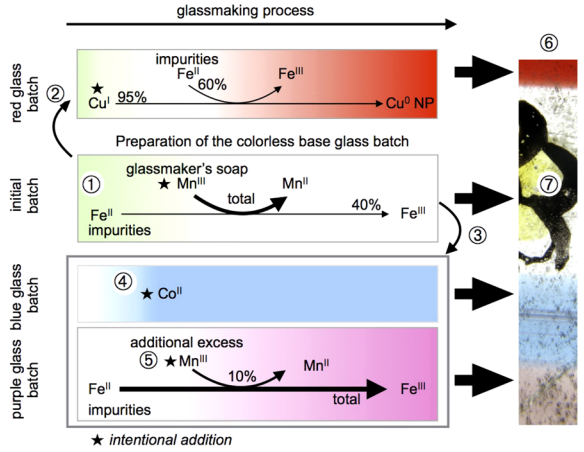

Figure 6. Summary scheme of the medieval striped glass making steps.

CONCLUSION

Nondestructive quantification of the TM redox, using PIXE−PIGE chemical mapping and optical absorption spectroscopy, allowed us for the first time to derive quantitative TM redox information from a complex medieval multicolored glass. These data revealed that the manganese concentration was carefully adjusted to control the redox processes of each color: (i) oxidation of divalent Fe to remove the greenish color of the base glass, (ii) the absence of oxidant manganese in the red stripe to allow the reduction of copper to metallic nanoparticles, and (iii) an excess of oxidized manganese in the purple stripe to obtain thermodynamically unstable trivalent manganese. Altogether, the comparison of the Fe, Cu, and Mn redox states demonstrates how medieval glassmakers mastered the thermodynamics and kinetics of the redox processes in the glass via mainly TM concentrations and fast glass shaping. Hence, this three-color striped glass appears to be the master piece of a medieval glass workshop, which illustrates the technical accomplishments performed at the end of the 15th century. This work demonstrates the possibility of achieving quantitative redox chemistry using nondestructive analytical methods in line with the recommended ethical guidelines for cultural heritage research.

ASSOCIATED CONTENT

Supporting Information

The Supporting Information is available free of charge on the ACS Publications website at DOI: 10.1021/acs.analchem.7b01452.

Examples of other European medieval striped glasses, extensive table of the chemical compositions of the blue, red, purple, and base glasses, details about the manganese−barium and manganese−iron correlations, and chemical mappings of the black staining (PDF)

AUTHOR INFORMATION

Corresponding Authors

*E-mail: myrtille.hunault@impmc.upmc.fr.
*E-mail: claudine.loisel@culture.gouv.fr.

ORCID

Myrtille O. J. Y. Hunault: 0000-0002-3754-8630

Present Address

⊥M.O.J.Y.H.: SOLEIL Synchrotron, l'Orme des merisiers Saint-Aubin BP48, 91192 Gif-Sur-Yvette Cedex, France.

Notes

The authors declare no competing financial interest.

ACKNOWLEDGMENTS

This work was supported by Sorbonne Universités, Convergence project "VITRAUX" (SU-14-R-ScPC-15-2).

DOI: 10.1021/acs.analchem.7b01452
Anal. Chem. 2017, 89, 6277−6284

REFERENCES

(1) Bamford, C. R. *Colour Generation and Control in Glass*; Elsevier Scientific Publishing Co.: Amsterdam, 1977.
(2) Janssens, K., Ed. *Modern Methods for Analysing Archaeological and Historical Glass*; John Wiley & Sons Ltd.: New York, 2013; pp i−xxv.
(3) Rehren, T.; Freestone, I. C. *J. Archaeol. Sci.* **2015**, *56*, 233−241.
(4) Kunicki-Goldfinger, J. J.; Freestone, I. C.; McDonald, I.; Hobot, J. A.; Gilderdale-Scott, H.; Ayers, T. *J. Archaeol. Sci.* **2014**, *41*, 89−105.
(5) Hunault, M.; Bauchau, F.; Loisel, C.; Hérold, M.; Galoisy, L.; Newville, M.; Calas, G. *J. Am. Ceram. Soc.* **2016**, *99*, 89−97.
(6) Bingham, P.; Jackson, C. *J. Archaeol. Sci.* **2008**, *35*, 302−309.
(7) Sellner, C.; Oel, H.; Camara, B. *Glastech. Ber.* **1979**, *52*, 255−264.
(8) Schreurs, J. W. H.; Brill, R. H. *Archaeometry* **1984**, *26*, 199−209.
(9) (a) Dran, J.-C.; Salomon, J.; Calligaro, T.; Walter, P. *Nucl. Instrum. Methods Phys. Res., Sect. B* **2004**, *219−220*, 7−15. (b) Morelle, M.; El Masri, Y.; Heitz, C.; Prieels, R.; Van Mol, J.; Dran, J. C.; Salomon, J.; Calligaro, T.; Dubus, M. *Nucl. Instrum. Methods Phys. Res., Sect. B* **2005**, *240*, 600−605. (c) Beck, L. *Nucl. Instrum. Methods Phys. Res., Sect. B* **2014**, *332*, 439−444.
(10) Nakai, I.; Numako, C.; Hosono, H.; Yamasaki, K. *J. Am. Ceram. Soc.* **1999**, *82*, 689−695.
(11) Farges, F.; Etcheverry, M.-P.; Scheidegger, A.; Grolimund, D. *Appl. Geochem.* **2006**, *21*, 1715−1731.
(12) Ferrand, J.; Rossano, S.; Loisel, C.; Trcera, N.; van Hullebusch, E. D.; Bousta, F.; Pallot-Frossard, I. *Anal. Chem.* **2015**, *87*, 3662−3669.
(13) Ceglia, A.; Nuyts, G.; Meulebroeck, W.; Cagno, S.; Silvestri, A.; Zoleo, A.; Nys, K.; Janssens, K.; Thienpont, H.; Terryn, H. *J. Anal. At. Spectrom.* **2015**, *30*, 1552−1561.
(14) Meulebroeck, W.; Cosyns, P.; Baert, K.; Wouters, H.; Cagno, S.; Janssens, K.; Terryn, H.; Nys, K.; Thienpont, H. *J. Archaeol. Sci.* **2011**, *38*, 2387−2398.
(15) Hunault, M.; Lelong, G.; Gauthier, M.; Gélébart, F.; Ismael, S.; Galoisy, L.; Bauchau, F.; Loisel, C.; Calas, G. *Appl. Spectrosc.* **2016**, *70*, 778−784.
(16) Meulebroeck, W.; Wouters, H.; Nys, K.; Thienpont, H. *Sci. Rep.* **2016**, *6*, 1−10.
(17) Mirti, P.; Davit, P.; Gulmini, M. *Anal. Bioanal. Chem.* **2002**, *372*, 221−229.
(18) Pichon, L.; Beck, L.; Walter, P.; Moignard, B.; Guillou, T. *Nucl. Instrum. Methods Phys. Res., Sect. B* **2010**, *268*, 2028−2033.
(19) Pichon, L.; Moignard, B.; Lemasson, Q.; Pacheco, C.; Walter, P. *Nucl. Instrum. Methods Phys. Res., Sect. B* **2014**, *318*, 27−31.
(20) Pichon, L.; Calligaro, T.; Lemasson, Q.; Moignard, B.; Pacheco, C. *Nucl. Instrum. Methods Phys. Res., Sect. B* **2015**, *363*, 48−54.
(21) Aubert, M.; Grodecki, L. *Les Vitraux de Notre-Dame et de la Sainte-Chapelle de Paris*; Corpus Vitrearum Medii Aevi 1; Caisse nationale des monuments historiques, Centre national de la recherche scientifique: Paris, 1959.
(22) De Raedt, I.; Janssens, K.; Veeckman, J.; Vincze, L.; Vekemans, B.; Jeffries, T. E. *J. Anal. At. Spectrom.* **2001**, *16*, 1012−1017.
(23) Maxwell, J. A.; Campbell, J. L.; Teesdale, W. J. *Nucl. Instrum. Methods Phys. Res., Sect. B* **1989**, *43*, 218−230.
(24) Lombardo, T.; Loisel, C.; Gentaz, L.; Chabas, A.; Verita, M.; Pallot-Frossard, I. *Corros. Eng., Sci. Technol.* **2010**, *45*, 420−424.
(25) Grieken, R. v.; Janssens, K. *Cultural Heritage Conservation and Environmental Impact Assessment by Non-Destructive Testing and Micro-Analysis*; Taylor and Francis: London, 2005.
(26) Calligaro, T. *X-Ray Spectrom.* **2008**, *37*, 169−177.
(27) Hunt, R. W. G.; Pointer, M. R. *Measuring Colour*, 4th ed.; John Wiley and Sons: New York, 2011.
(28) Henderson, J. *The Science and Archaeology of Materials: An Investigation of Inorganic Materials*; Rutledge: New York, 2000.
(29) Schalm, O.; Janssens, K.; Wouters, H.; Caluwé, D. *Spectrochim. Acta, Part B* **2007**, *62*, 663−668.
(30) Jackson, C. M.; Smedley, J. W. *Glass Technol.: Eur. J. Glass Sci. Technol., Part A* **2004**, *45*, 36−42.
(31) Jackson, C. M.; Booth, C. A.; Smedley, J. W. *Archaeometry* **2005**, *47*, 781−795.
(32) Moretti, C.; Hreglich, S. In *Modern Methods for Analysing Archaeological and Historical Glass*; Janssens, K., Ed.; John Wiley & Sons Ltd.: New York, 2013; pp 23−47.
(33) Brill, R. H. *Int. Congr. Glass, Artistic Hist. Commun., 9th* **1972**, 93−110.
(34) Radepont, M.; Lemasson, Q.; Pichon, L.; Moignard, B.; Pacheco, C. *Measurement* **2016**, DOI: 10.1016/j.measurement.2016.07.005.
(35) De Raedt, I.; Janssens, K.; Veeckman, J. *J. Anal. At. Spectrom.* **1999**, *14*, 493−498.
(36) Velde, B. In *Modern Methods for Analysing Archaeological and Historical Glass*; Janssens, K., Ed.; John Wiley & Sons Ltd.: New York, 2013; pp 67−78.
(37) Freestone, I. C. Theophilus and the Composition of Medieval Glass. Symposium J - Materials Issues in Art and Archaeology III; 1992.
(38) Bontemps, G. *Guide du verrier: traité historique et pratique de la fabrication des verres, cristaux, vitraux*; Librairie du Dictionnaire des arts et manufactures: Paris, 1868.
(39) Jackson, C. M. *Archaeometry* **2005**, *47*, 763−780.
(40) Gratuze, B.; Soulier, I.; Barrandon, J. N.; Foy, D. *Trade and Discovery: The Scientific Study of Artefacts from Post-Medieval Europe and Beyond* **1995**, 123−33.
(41) Hunault, M.; Calas, G.; Galoisy, L.; Lelong, G.; Newville, M. *J. Am. Ceram. Soc.* **2014**, *97*, 60−62.
(42) Möncke, D.; Papageorgiou, M.; Winterstein-Beckmann, A.; Zacharias, N. *J. Archaeol. Sci.* **2014**, *46*, 23−36.
(43) Wagner, F. E.; Haslbeck, S.; Stievano, L.; Calogero, S.; Pankhurst, Q. A.; Martinek, K.-P. *Nature* **2000**, *407*, 691−692.
(44) Lafait, J.; Berthier, S.; Andraud, C.; Reillon, V.; Boulenguez, J. *C. R. Phys.* **2009**, *10*, 649−659.
(45) Haiss, W.; Thanh, N. T. K.; Aveyard, J.; Fernig, D. G. *Anal. Chem.* **2007**, *79*, 4215−4221.
(46) Schreiber, H. D.; Kozak, S. J.; Balazs, G. B.; Fritchman, A. L.; Schreiber, C. W. *J. Am. Ceram. Soc.* **1989**, *72*, 1680−1691.
(47) Schreiber, H. D. *J. Non-Cryst. Solids* **1986**, *84*, 129−141.
(48) Chopinet, M.-H.; Lizarazu, D.; Rocanière, C. *C. R. Chim.* **2002**, *5*, 939−949.
(49) Arletti, R.; Dalconi, M. C.; Quartieri, S.; Triscari, M.; Vezzalini, G. *Appl. Phys. A: Mater. Sci. Process.* **2006**, *83*, 239−245.
(50) Quaranta, A.; Ceccato, R.; Menato, C.; Pederiva, L.; Capra, N.; Dal Maschio, R. *J. Non-Cryst. Solids* **2004**, *345−346*, 671−675.
(51) Lipinska-Kalita, K. E.; Krol, D. M.; Hemley, R. J.; Mariotto, G.; Kalita, P. E.; Ohki, Y. *J. Appl. Phys.* **2005**, *98*, 054301.
(52) Molina, G.; Murcia, S.; Molera, J.; Roldan, C.; Crespo, D.; Pradell, T. *J. Nanopart. Res.* **2013**, *15*, 1932.
(53) Pradell, T.; Pavlov, R. S.; Carolina Gutiérrez, P.; Climent-Font, A.; Molera, J. *J. Appl. Phys.* **2012**, *112*, 054307.
(54) Pérez-Villar, S.; Rubio, J.; Oteo, J. L. *J. Non-Cryst. Solids* **2008**, *354*, 1833−1844.
(55) Jembrih-Simbürger, D.; Neelmeijer, C.; Schalm, O.; Fredrickx, P.; Schreiner, M.; De Vis, K.; Mäder, M.; Schryvers, D.; Caen, J. *J. Anal. At. Spectrom.* **2002**, *17*, 321−328.
(56) Doyle, W. T. *Phys. Rev.* **1958**, *111*, 1067−1072.
(57) Lautier, C.; Sandron, D. *Antoine de Pise: l'art du vitrail vers 1400*; Comité des travaux historiques et scientifiques: Paris, 2008.
(58) Pradell, T.; Molina, G.; Murcia, S.; Ibáñez, R.; Liu, C.; Molera, J.; Shortland, A. J. *Int. J. Appl. Glass. Sci.* **2016**, *7*, 41−58.
(59) Hunault, M. O. J. Y.; Vinel, V.; Cormier, L.; Calas, G. *J. Am. Ceram. Soc.* **2017**, DOI: 10.1111/jace.14819.
(60) Hérold, M. *Revue de l'art* **2016**, *194*, 23−32.

DOI: 10.1021/acs.analchem.7b01452
Anal. Chem. 2017, 89, 6277−6284